Physica E 145 (2023) 115479

Contents lists available at ScienceDirect

Physica E: Low-dimensional Systems and Nanostructures

journal homepage: www.elsevier.com/locate/physe

# Advanced tunability of optical properties of CdS/ZnSe/ZnTe/CdSe multi-shell quantum dot by the band edge engineering

Fatih Koç [a], Ahmet Emre Kavruk [b], Mehmet Sahin [c,*]

[a] Department of Metallurgical and Materials Engineering, Ahi Evran University, Kırşehir, Turkey
[b] Physics Department, Faculty of Sciences, Selcuk University, Konya, Turkey
[c] Department of Nanotechnology Engineering, Abdullah Gul University, 38080 Kayseri, Turkey

ARTICLE INFO

*Keywords:*
Multi-shell quantum dot
Exciton transitions
Band edge engineering
Exciton lifetimes

ABSTRACT

In this study, the advanced manipulability of wave functions in a type-II multi-shell hetero-nanostructure (MS-HNS) and the tunability of radiative exciton lifetime over a wide range with and/or without changing in transition energies has been demonstrated by the band edge engineering. For this purpose, the electronic and optical properties of exciton (X) and biexciton (XX) in a spherical CdS/ZnSe/ZnTe/CdSe HNS have been explored in detail. In the calculations, effects of all Coulombic interactions between the charges have been taken into account on the wave functions. Moreover, in the case of XX, the exchange–correlation potential between the same charged particles has also been considered. The results have been presented as a function of CdS core radius and ZnSe shell thickness and the probable physical reasons have been discussed in detail.

## 1. Introduction

The core/shell hetero-nanostructures (HNSs) are stood out amongst other HNSs due to their adjustable parameters. These parameters, size, geometry, and material-dependent tunable electronic and optical properties, have played a key role in many application areas such as quantum dot lasers [1–3], light-emitting diodes (LEDs) [4–6], photovoltaic devices [7–9], biological imaging [10,11], and spintronics [12,13]. The electronic and optical properties of core/shell HNSs are mostly controlled by spatial distribution and confinement region size of the electrons and holes. In type-I core/shell HNSs, the electrons and holes are confined in the same spatial region. This confinement regime provides higher quantum efficiency [14] and quantum coherency [15] and due to these properties, type-I structures are preferred in, for example, fabrication of LEDs. If the charges are confined in the different spatial regions, this confinement regime is called type-II core/shell HNSs. In this confinement regime, the electronic energy levels of the charges can be separately tuned as desired by changing the size of the confinement regions [16–18]. This degree of freedom has paved the different ways for quantum core/shell HNSs to use in many new application areas.

Studies on type-I core/shell HNSs continue increasingly in various application areas due to their strong confinement effect and quantum coherency as mentioned above. One of the latest works shows that, field-effect transistors can achieve a sensitive photodetection ability by using type-I CdSe/CdS core/shell HNSs [19]. Another work demonstrates that the fabrication of the floating gate nonvolatile memory based on type-I quantum dots (QDs) can be possible with a large memory window, stable retention, and good endurance [20]. The resistive switching memory is another innovative application area of type-I core/shell HNSs [21]. In addition to all these, as is well known, the type-I core/shell HNSs are preferred in LED, water splitting [22], laser and quantum computing applications [23–25].

As for type-II core/shell HNSs, they are more appropriate structures for photovoltaics [16,26] due to lower recombination rates depending on charge separation. On the other hand, Kim et al. [27] demonstrated that the recombination quantum efficiency can be increased somewhat in type-II structures. Thus, the fabrication of type-II based QDLEDs has been carried out, even if it has not too much quantum efficiency when compared to the type-I counterpart. It is reported that these type-II QDLEDs work mostly in the near-infrared region, effectively [28]. Another remarkable application area is that a high-fidelity optical quantum gate can be obtained using type-II double QDs [29].

Designing multi-shell HNSs can take the degree of freedom on the tunability one step further when compared to type-II structures and these structures can be used for many different purposes [30–33]. Experimentally, multi-shell HNSs can be fabricated successfully via many physical and chemical growth techniques such as, successive ionic layer adsorption and reaction (SILAR) [22,34,35]. As is mentioned above, as well as tunability of quantum efficiency in type-II structures, the binding energies, and overlap of wave functions can be manipulated

* Corresponding author.
*E-mail address:* mehmet.sahin@agu.edu.tr (M. Sahin).

https://doi.org/10.1016/j.physe.2022.115479
Received 12 April 2022; Received in revised form 26 August 2022; Accepted 27 August 2022
Available online 5 September 2022

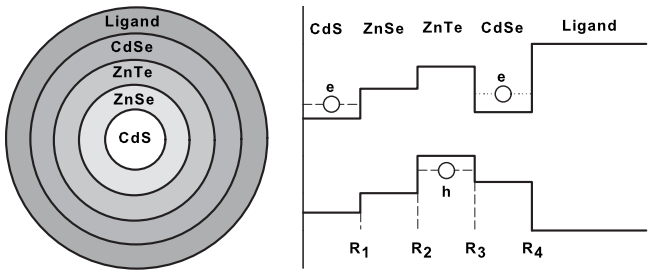


**Fig. 1.** Representation of CdS/ZnSe/ZnTe/CdSe HNS and its potential profile. While the hole is confined into the ZnTe shell, the electron can be confined in CdS core or CdSe shell depending on the sizes.

more effectively [18,30,36]. Moreover, in the multi-shell HNSs, more than one confinement region can be formed and particles can be confined in the desired region by means of changing the size of shells or other tunable material parameters. All these control mechanisms open a new door of advanced wave function engineering in HNSs. Thanks to wave function engineering, a switching between type-I and type-II localization regimes can be tuned more effectively [31]. With these properties, multi-shell HNSs can be used in quantum memory devices [37]. After all, multi-shell HNSs may be the most suitable candidate for the main component of future hi-tech novel devices, because they provide opportunities for new possibilities via their more tunable key features.

The main purpose of this study is to show the independent controllability from one another of transition energies and radiative lifetimes of exciton and biexciton in multi-shell quantum dot structures. This independent tunability over transition energies and lifetimes is not possible in single core/shell quantum dot structures. From this point of view, the results of the study are thought it is able to be extremely critical in terms of electro-optical device applications. In order to demonstrate this independent tunability, here, a spherical CdS/ZnSe/ZnTe/CdSe multi-shell QD is considered. In this multi-shell QD, holes have been confined in the ZnTe shell because of the lowest confinement potential for all CdS core and ZnSe shell thickness. On the other hand, the electron can be localized mostly in CdS or CdSe depending on their sizes. Therefore, the electronic and optical properties have been investigated for different CdS core radius and ZnSe shell thickness. The obtained results are presented as a function of ZnSe thicknesses for different core sizes.

## 2. Model and theory

Here, we have considered a spherically symmetric CdS/ZnSe/ZnTe/CdSe multi-shell HNS. Schematic representation and potential profile of the structure are given in Fig. 1.

The electronic states and corresponding wave functions have been determined by the self-consistent solution of Poisson–Schrödinger equations. In the effective mass approximation and BenDaniel–Duke boundary conditions [38], the single-particle radial Schrödinger equation of the electron and hole for the ground state is given by [39]:

$$\left[-\frac{\hbar^2}{2}\vec{\nabla}_r\left(\frac{1}{m_e^*(r)}\vec{\nabla}_r\right)+V_e(r)-q_e\Phi_h+q_e\Phi_e+V_{xc}^{e-e}[\rho_e(r)]\right]R_e(r) = \varepsilon_e R_e(r), \tag{1}$$

and

$$\left[-\frac{\hbar^2}{2}\vec{\nabla}_r\left(\frac{1}{m_h^*(r)}\vec{\nabla}_r\right)+V_h(r)-q_h\Phi_e+q_h\Phi_h+V_{xc}^{h-h}[\rho_h(r)]\right]R_h(r) = \varepsilon_h R_h(r). \tag{2}$$

Here, $e$ and $h$ are symbolize the electron and hole, respectively, $\hbar$ is the reduced Planck constant, $m_{e,h}^*(r)$ is the position-dependent effective mass of the particles, $V_{e,h}(r)$ is the confinement potential, $q_{e,h}$ is charge of the particles, $\Phi_{e,h}$ is the electrostatic Coulomb potential of the particle, $V_{xc}^{e-e}$ and $V_{xc}^{h-h}$ are the exchange–correlation potentials between the same particles, $R_{e,h}(r)$ is the radial wave functions and $\varepsilon_{e,h}$ is the energy eigenvalues. These equations contain the repulsive Coulomb and exchange–correlation terms caused by particles with the same charges for the case of more than one electron (hole). Hence, for single electron/hole calculations, the repulsive Coulomb and exchange–correlation terms are taken as zero.

These two separated equations become a coupled equation thanks to the attractive Coulomb terms ($q_e\Phi_h$ and $q_h\Phi_e$) between the electron and hole. In the first step, all of the attractive and repulsive electrostatic Coulomb terms are taken as zero and the energy levels and the corresponding wave functions of the electron and hole are calculated without any interaction. In the second step, using obtained wave functions in the first step, the electrostatic Coulomb terms of the electron and hole are calculated from the following Poisson equations [39],

$$\vec{\nabla}\kappa(r)\vec{\nabla}\Phi_e = q_e\rho_e(r), \qquad \vec{\nabla}\kappa(r)\vec{\nabla}\Phi_h = -q_h\rho_h(r), \tag{3}$$

where, $\kappa(r)$ is the dielectric constant of the material, $\rho_e$ and $\rho_h$ are the density of the electron and hole [40]. In the next step, these electrostatic Coulomb terms are substituted into Eqs. (1) and (2) and these 3 steps are repeated until the desired convergence is achieved. After all these steps, the final energies and the corresponding wave functions of the electron and hole are obtained. The electronic and optical properties of the CdS/ZnSe/ZnTe/CdSe multi-shell HNS are calculated from these final energies and wave functions of the electron and hole.

In the HNSs, since the confinement effect of the structure, the attractive Coulomb potential between the electron and hole becomes more powerful and effective. Therefore, the hole and electron move as if a single particle called an exciton. The total energy of the exciton determines the absorption frequency (transition energy) and this total energy strongly depends mostly on the size of the shells of the HNS. For an excitonic formation, the total energy is expressed as [40],

$$E_X^{tot/tr} = E_g + \varepsilon_e + \varepsilon_h - \varepsilon_{e-h} \tag{4}$$

here, $E_g$ is bandgap energy of the confinement region, $\varepsilon_e$, and $\varepsilon_h$ are the energy eigenvalues of the electron and hole, respectively, and $\varepsilon_{e-h}$ is the attractive Coulomb energy between the electron and hole. As can be seen from Eqs. (1) and (2), since the $\varepsilon_{e-h}$ is included separately in both the electron and hole energies, one of them must be subtracted from the total energy [40].

The binding energy is an important parameter for device applications and it also plays an active role in determining the optical properties. For a single exciton, the binding energy is equal to the attractive Coulomb energy between the electron and hole and it is calculated by means of [40]

$$E_B(X) = E_g + \varepsilon_e^0 + \varepsilon_h^0 - E_X^{tot}, \tag{5}$$

here, $\varepsilon_e^0$ and $\varepsilon_h^0$ are the electron and hole energies that are determined without Coulomb interaction at the first step.

As is well known, more than one electron and/or hole can be confined in HNSs. If there are two electrons and two holes in HNSs, this formation called a biexciton. The total energy of a biexciton can be written as,

$$E_{XX}^{tot} = 2E_g + E_{elec}^{tot} + E_{hole}^{tot} - \varepsilon_{e-h} - \frac{q_e}{2}\int\phi_e\rho_e(r)d^3r - \frac{q_h}{2}\int\phi_h\rho_h(r)d^3r + E_{xc}^{e-e}[\rho_e(r)] - \int\rho_e(r)V_{xc}^{e-e}d^3r + E_{xc}^{h-h}[\rho_h(r)] - \int\rho_h(r)V_{xc}^{h-h}d^3r, \tag{6}$$

where $E_{elec}^{tot}$ and $E_{hole}^{tot}$ are the total energies of electrons and holes, $E_{xc}^{e-e}[\rho_e(r)]$ and $E_{xc}^{h-h}[\rho_h(r)]$ are the density dependent exchange–correlation energies of the electrons and holes, $V_{xc}^{e-e}$ and $V_{xc}^{h-h}$ are the

exchange–correlation potentials of the electrons and holes, respectively. These terms are discussed in detail in our previous work [36].

In the single exciton case, transition energy is equal to the total energy of the exciton. But in the case of biexciton, transition energy, $E_{tr}$, is defined as

$$E_{XX}^{tr} = E_{XX}^{tot} - E_{X}^{tot}. \tag{7}$$

The binding energy of the biexciton can be calculated by means of [41],

$$E_B(XX) = 2E_X^{tot} - E_{XX}^{tot}. \tag{8}$$

Overlap between the wave functions of the electron and hole is a decisive parameter on the recombination lifetime. In type-I HNSs, since the electron and hole are confined in the same spatial region, manipulation of the shell size has the nearly same effect on the electron and hole wave functions. Therefore in type-I HNSs, the shell size has a limited effect on the overlap. On the other side, in type-II HNSs, the electron and hole can be confined in different spatial regions, and as a result of this, the overlap can be adjusted in a wide range with manipulation of the shell sizes. The overlap integral is expressed as [42],

$$\theta(X) = \left| \int r^2 dr R_e^X(r) R_h^X(r) \right|^2 \tag{9}$$

$$\theta(XX) = \left| \int r^2 dr R_e^{XX}(r) R_h^{XX}(r) \right|^2 \tag{10}$$

here, $R_e^{X(XX)}(r)$ and $R_h^{X(XX)}(r)$ are the radial wave functions of the electron and hole, respectively, for the exciton (biexciton). In order to define the optical transitions, a unitless quantity called oscillator strength is used and for the exciton and biexciton, it can be expressed as follows, respectively [43],

$$f_X = \frac{E_p}{2E_X^{tr}} \theta(X), \tag{11}$$

$$f_{XX} = A \frac{E_p}{2E_{XX}^{tr}} \theta(XX). \tag{12}$$

Here, $E_p$ is the Kane energy, A is a recombination probability factor, and $A \simeq 2$ for the unbound biexciton and $A \simeq 4$ [44] for the bound biexciton.

The radiative lifetime is given as [45],

$$\tau = \frac{6\pi\varepsilon_0 m_0 c^3 \hbar^2}{e^2 n \beta_s E^2 f}, \tag{13}$$

where $\varepsilon_0$ is the dielectric permittivity of the vacuum, $m_0$ is the free electron mass, $c$ is the velocity of light in vacuum, $e$ is the electronic charge, $f$ is the oscillator strength, $n$ is the refractive index, $E$ is the transition energy and $\beta_s$ is the screening factor [46], which can be written as,

$$\beta_s = \frac{3\varepsilon}{\varepsilon_{HNS} + 2\varepsilon}. \tag{14}$$

Here, $\varepsilon$ and $\varepsilon_{HNS}$ optical dielectric constants of the medium and HNS, respectively.

## 3. Results and discussion

In this study, CdS/ZnSe/ZnTe/CdSe multi-shell HNS has been considered as a function of the ZnSe shell thickness at different core radii. In the calculations, the atomic units have been used, $\hbar = m_0 = e = 1$, and ZnTe and CdSe shells size set to 0.25 $a_0^*$. The effective exciton Bohr radius, $a_0^*$, and the effective Rydberg energy have been calculated based on CdS parameters and their values are 28.9 Å and 28.6 meV, respectively. The material parameters used in the calculations have been given in Table 1. It should be noted that, in the literature, there are a number of studies related to the effect of ligands on the electronic and optical properties of QDs [47–49]. In these studies, it is reported that these effects may be important and hence, in this study, the ligand effect has also been taken into account in the calculations.

**Table 1**
Material parameters.

| | CdS | ZnSe | ZnTe | CdSe | Ligand |
|---|---|---|---|---|---|
| $m_e^*$ | 0.2 [50] | 0.16 [50] | 0.122 [50] | 0.12 [50] | 1.0 [51] |
| $m_h^*$ | 0.8 [50] | 0.75 [50] | 0.6 [50] | 0.45 [50] | 1.0 [51] |
| $\kappa$ | 8.73 [50] | 8.60 [50] | 10.3 [50] | 9.29 [50] | 2.0 [48] |
| $V_e$ (eV) | | 0.8 [52] | 0.59 [53] | 1.22 [52] | 3.0 |
| $V_h$ (eV) | | 0.52 [52] | 1.0 [53] | 0.7 [52] | 3.0 |

In the CdS/ZnSe/ZnTe/CdSe multi-shell HNS, as shown in Fig. 1, there are two confinement regions for the electron while the hole is localized only into the ZnTe shell. Owing to this confinement region alignment, the optical and electrical properties can exhibit both quasi-type-I and type-II confinement regimes according to shell thickness. In the case of small core sizes, the electron density is expanded to the whole structure and it behaves like quasi type-I confinement. As the size of the core increases, the electron is confined completely in the core region and the structure exhibits an orthodox type-II confinement regime due to the spatial distance between the electron and hole. On the other hand, with this structure, it is aimed to demonstrate the possibility of the manipulation of both binding energies and overlap integrals in a wide range without notable changes in the energies of the particles. For this purpose, we have specifically focused on the thickness change of the ZnSe shell which is between the electron and the hole's confinement region.

Fig. 2 depicts the total energy of the exciton and biexciton as a function of the ZnSe shell thickness for different core radii. As seen from the figure, the total energies are monotonically decreasing in the vertical direction with the increasing core size as expected. On the other hand, there are no notable changes in the energies with the increasing ZnSe shell thickness and this is important for device applications like photovoltaic devices. These changes can be explained by means of finding probability of the charges. As shown in Fig. 3, for the core radius 0.275 $a_0^*$, because of its higher kinetic energy, the electron can easily tunnel into the CdSe shell which is the second well. From another point of view, the density of the electron spreads throughout the whole structure so the electron behaves as if in a single potential well with a perturbed from the bottom as can be seen in Fig. 3. Hence, the total energy of the exciton decreases with increasing the ZnSe shell thickness. On the other hand, when we focus on the right side of Fig. 2, we see that the changes in the biexciton total energies with the ZnSe thickness are much lesser than that of the exciton. This behaviour can be attributed to the repulsive Coulomb interaction between the same charged particles. But, as the core radius continues to increase, the electron density begins to be drawn into the core region. In the bigger core radius cases, when the ZnSe shell thickness reaches a certain value, the total energy of the biexciton rises slightly since the repulsive interactions become predominant.

The binding energies are important quantities in understanding the formation of quantum mechanical systems. As well known, in most of many particles quantum systems, there can be a lot of interactions, like Coulomb, exchange–correlation, etc., that have effects on the binding energy. Among them, the Coulomb interactions are more dominant and bound structures are formed when the Coulomb interactions are attractive. In Fig. 4, the binding energies for both X and XX structures are demonstrated. The binding energy of an exciton is equal to attractive Coulomb energy only between the charges and hence its magnitude is strongly dependent on the spatial distance of the charges. As seen in Fig. 3, an increase in the thickness of ZnSe leads to larger charge separations. Because of this fundamental physical reason, as can be seen from Fig. 4, the binding energy of the exciton decreases with increasing ZnSe thickness. On the other hand, the biexciton exhibits different

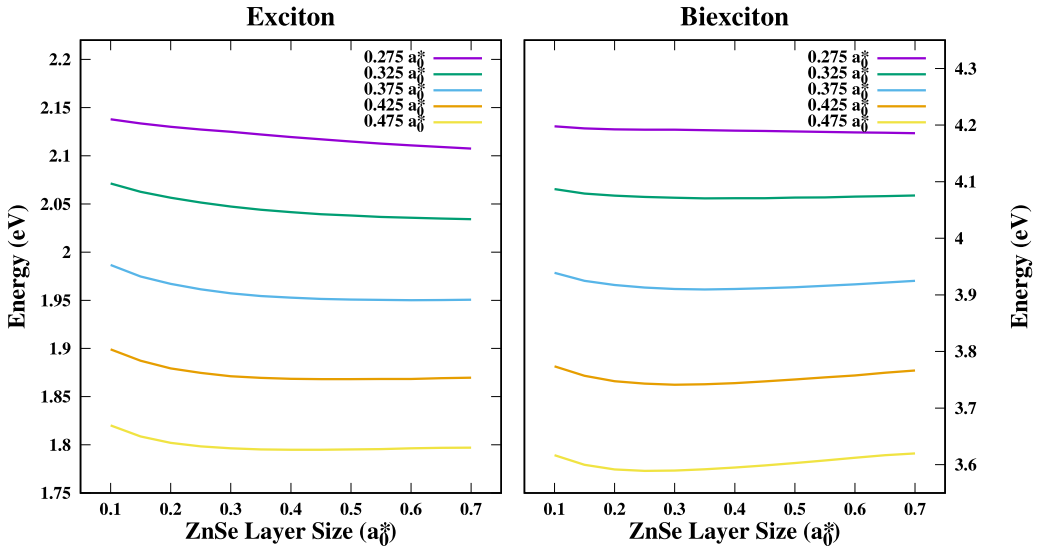


**Fig. 2.** Total energies of the exciton and biexciton as a function of the ZnSe shell size for different core radii.

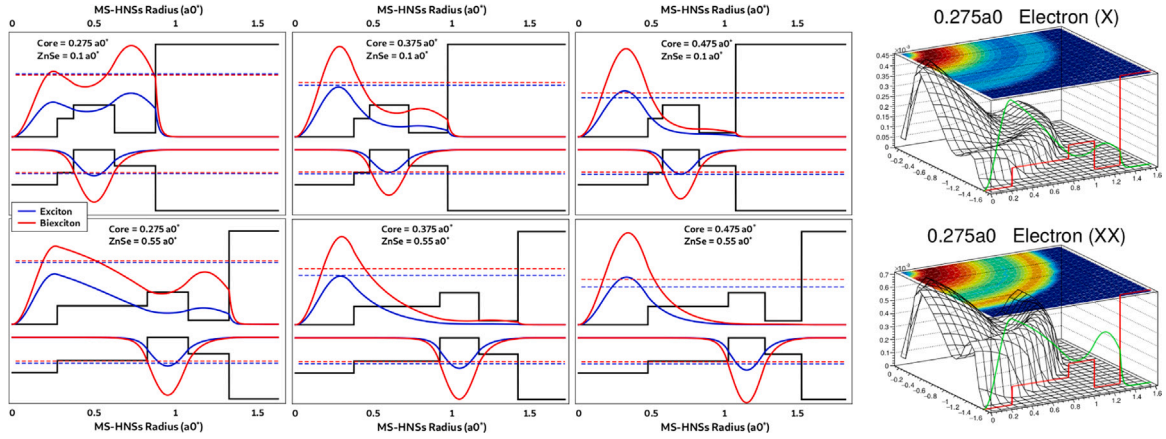


**Fig. 3.** Densities of the electron and hole for the exciton (red) and biexciton (blue) cases for 0.55 $a_0^*$ ZnSe shell size at different core radii. The 3D figure in the right panel is for a better view of the distribution of electron densities in X and XX.

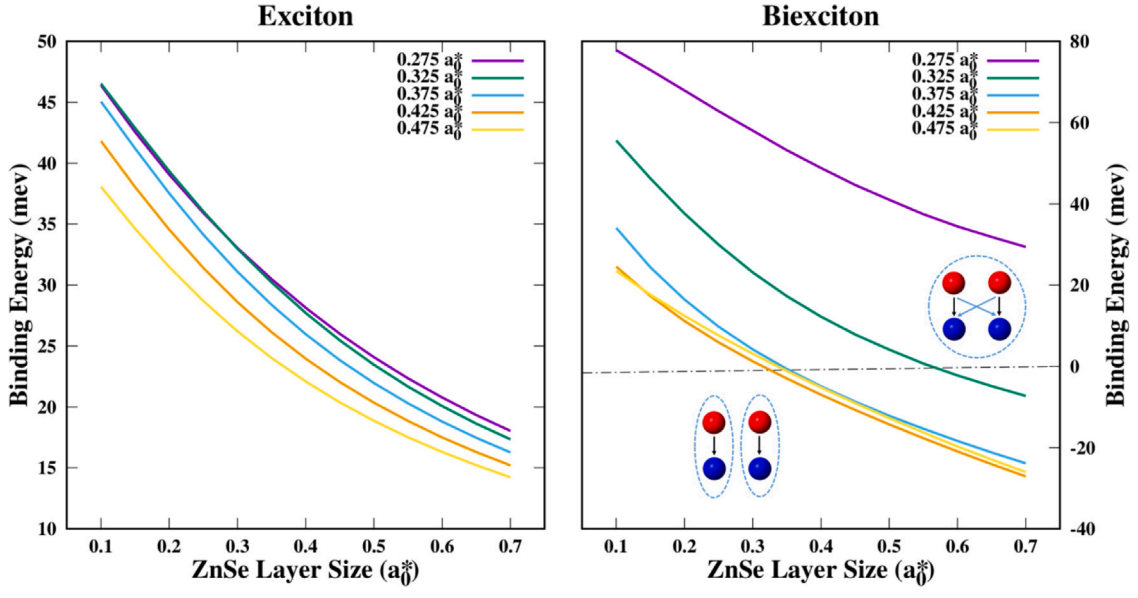


**Fig. 4.** Binding energies of the exciton and biexciton as a function of the ZnSe shell thickness for different core radii. The negative values in the biexciton binding energies correspond to unbound cases. In right panel, the upper and lower insets illustrate bound and unbound biexciton cases, respectively.

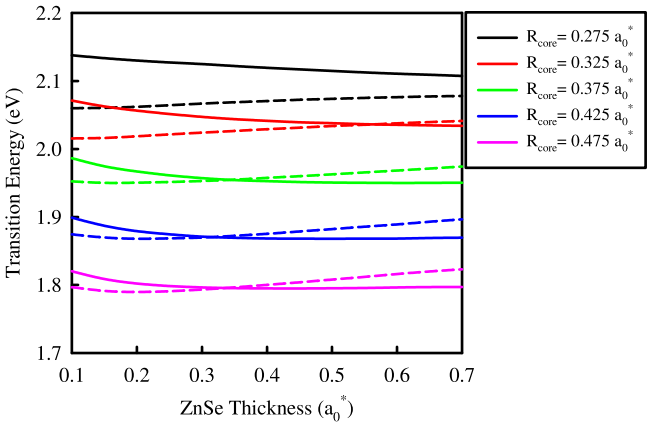


**Fig. 5.** Transition energies of exciton (solid lines) and biexciton (dashed lines) as a function of ZnSe thickness for different core radii.

behaviour depending on the magnitudes of attractive and repulsive interactions. If the attractive Coulomb effect overcomes the repulsive one, two electrons and two holes move together like a single particle (top inset in the right panel of Fig. 4) and it is named as a bound biexciton. If the repulsive Coulomb effect is dominant, two excitons move separately (bottom inset in the right panel of the figure) and this structure is called an unbound biexciton. As seen from Fig. 4, the binding energy of the biexciton is positive at all values of the ZnSe shell for the core radius 0.275 $a_0^*$. This means that the bound biexcitonic structure is formed in which the attractive Coulomb effect is dominant. When we look at the density of the electron and hole in Fig. 3, we see that the electron density invades the whole structure for the core radius of 0.275 $a_0^*$ and the attractive Coulomb is stronger because of the smaller spatial distance between the electrons and holes. At large core radii, as mentioned above, the electron is confined mostly in the core and this leads to weakened attractive Coulomb interaction with increasing ZnSe thickness.

The transition energies are another important parameter especially for technological applications of QDs such as photovoltaic devices. In most device applications, there can be some issues for the desired device fabrication depending on the transition energies. For example, in solar cell applications, either the exciton lifetime can be shorter relatively in appropriate working wavelength (i.e transition energy) or vice versa. Fig. 5 demonstrates the changing transition energies of X and XX with ZnSe thickness for different core radii. The transition energies can be tuned depending on the core radius and at each core radius, the X and XX transition energies are close to each other as expected [54–56]. On the other hand, while the transition energies remain almost the same with increasing ZnSe shell thickness, other optical properties, such as radiative lifetime, are changing. This is very important in terms of the controllability of the optical properties. In the figure, the XX transition energies are lower than that of the X especially for smaller core radii and ZnSe shell thicknesses. It should be noted that these cases correspond to the bound XX structures. On the other hand, beyond the certain ZnSe thickness, the biexciton transition energy is crossing the exciton transition energy and becomes larger with a further increase in the shell thickness. It is seen that this crossing occurs at smaller thicknesses when core radii increase. These cases correspond to unbound XX structures.

In order to see more explicitly the crossing mentioned in the discussion of Fig. 5, the absorption line-shapes in arbitrary units have been plotted in Fig. 6. Here, the line shape can be given by a Lorentzian curve which is expressed as

$$\delta_{X(XX)} = \frac{1}{\pi\hbar\Gamma} sech\left(\frac{E^{tr}_{X(XX)} - \hbar\omega}{\hbar\Gamma}\right). \quad (15)$$

Here, $\hbar\omega$ is incident photon energy and $\hbar\Gamma$ is line-shape broadening factor, taken as 30 meV. In the figure, when the core radius is 0.275 $a_0^*$, exciton absorption energies are higher than that of biexciton for all ZnSe shell thicknesses. However, the difference between the transition energies of X and XX decreases with increasing shell thickness. On the other hand, the difference between the transition energies is decreasing with increasing core radius and the transition energy becomes larger for XX with further increasing of ZnSe shell thickness at the greater core radii. It should be noted that the differences are very small as reported in experimental studies as well [54–56] and we conclude that the results are in a good agreement with the experimental studies as tendency [57].

The overlap integral has a decisive role on the optical properties. In type-I HNSs, the overlap integral values do not become smaller than 0.7 mostly while it can approaches zero in type-II counterparts. This wide range wave function engineering enables these structures to come to the fore in different application areas. As shown in Fig. 7, the overlap integrals of the exciton and the biexciton can be controlled between 0.70 and almost 0.0 depending on the core radius and ZnSe thickness. When we assess Fig. 7 comparing with Fig. 5 as a function of ZnSe thickness, we see that the transition energy is almost the same for a certain core radius, but the overlap can be changed in a wide range. This means the optical properties can be adjusted without dramatic changes in transition energies. At the same time, similar control can be performed as well by changing the core size at certain ZnSe shell thicknesses. It should be noted that these kinds of controls are not possible in bare type- I or type-II structures. This is a perfect example for advanced wave function engineering and hence, this controllable degree of freedom is very important especially for electro-optic device applications. With this feature, such structures are expected to offer great convenience for device applications.

The radiative lifetime, directly related to the overlap integral (Eq. (13)), can be measured experimentally as well and is a key parameter in the optical characterization of quantum dot nanocrystals and also device applications. The radiative lifetime of the exciton and biexciton in HNSs are generally in the order of a few nanoseconds. While the lifetime cannot be tuned in a wide range in type-I structures, it can be performed in type-II regions relatively but still not in a wide range and other properties are also changing such as transition energies. On the other hand, the radiative lifetime in multi-shell type-II HNSs especially can be increased significantly thanks to advanced wave function engineering opportunities as it has been discussed in Fig. 7. Moreover, in this controllability, there are no drastic changes in transition energies as well. This is an excellent success of wave function engineering in multi-shell HNSs. As is well known, since higher recombination probability, the radiative lifetime of the biexciton is shorter than that of the exciton [44,58]. In addition, in our previous study [44], we showed that the recombination probability of a bound biexciton is 2 times larger than that of the unbound one. This means the radiative lifetime of the unbound biexciton is 2 times longer than that in the bound one as the lifetime is inversely proportional to the recombination probability. Fig. 8 shows the radiative recombination lifetime of the exciton and biexciton as a function of the ZnSe shell thicknesses at different core radii. As expected, in all cases, the exciton lifetime is longer than that of the biexciton. In smaller core radii, the structure exhibits quasi type-I confinement regime and the lifetime for both X and XX becomes smaller and with increasing core radii the lifetimes become longer due to type-II confinement regime. Controlling of core radii gives an opportunity for tuning both lifetime and transition energies and in calculations, we see that the lifetime can be adjusted almost between 4–70 times. On the other hand, without changing transition energies, controlling the lifetime for both X and XX is possible in a range between 4–50 times by changing ZnSe thickness. In overall, the radiative lifetime for both X and XX can be controlled in a wide region between 4–200 times roughly by changing both core size and ZnSe thickness.

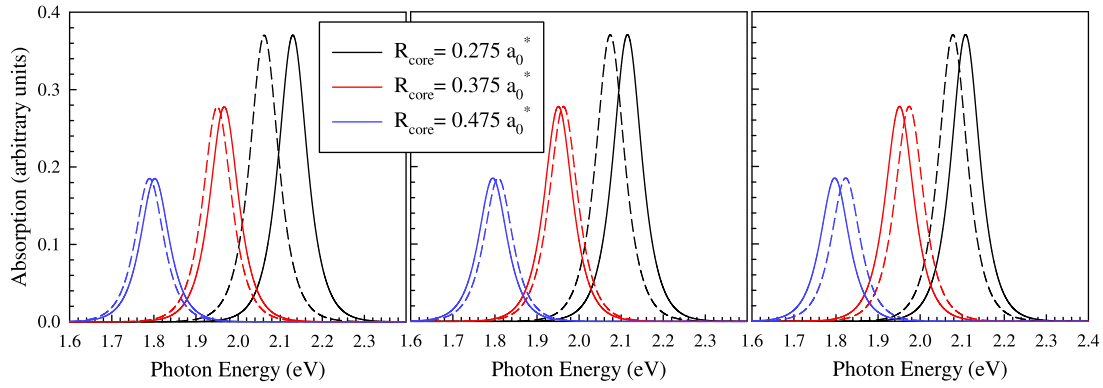


**Fig. 6.** The absorption line shape of X (solid lines) and XX (dashed lines) as a function of incident photon energy for ZnSe shell thickness of 0.2 $a_0^*$ (left panel), 0.5 $a_0^*$ (middle panel), and 0.7 $a_0^*$ (right panel). Here, each line colour corresponds the same core radius in all panels.

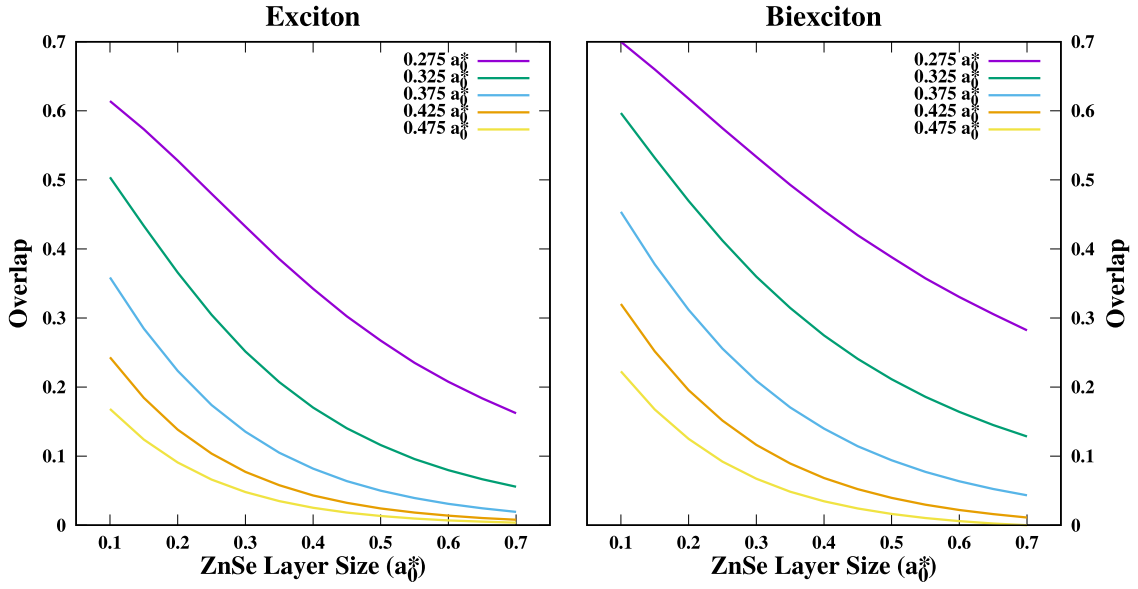


**Fig. 7.** Variation of the overlap integral of the exciton and biexciton with increasing ZnSe shell size for different core radii.

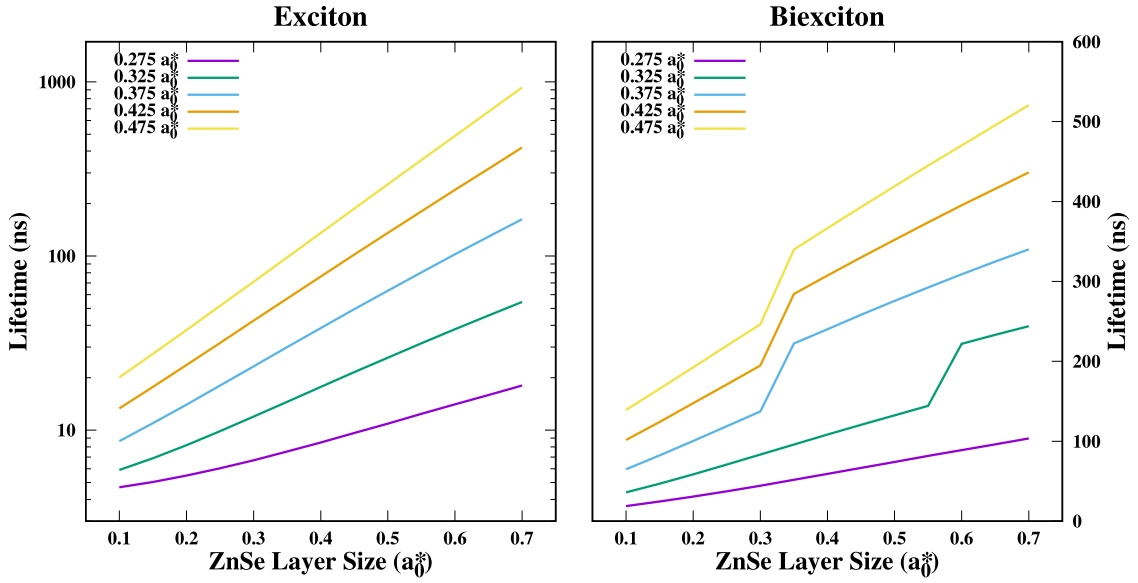


**Fig. 8.** The radiative lifetime of the exciton and biexciton as a function of the ZnSe shell size for different core radii.

## 4. Conclusion

In conclusion, we have carried out a detailed investigation of the electronic and optical properties of exciton and biexciton in CdS/ZnSe/ZnTe/CdSe multi-shell HNS as a function of both CdS core and ZnSe shell sizes. We have shown that CdS core radius plays a critical role in the electronic and optical properties of the exciton and biexciton in this multi-shell HNS via determining the localization region of the electron. Besides, we observed that ZnSe shell size can be used as a sensitive overlap manipulation tool and overlap between the electron and hole wave functions can be tuned in a wide range with the almost unchanged transition energy of the exciton and biexciton. As a result, we demonstrated the advanced manipulability of wave functions in type II multi-shell HNS and the tunability of radiation lifetime over a huge region without drastic changes in transition energies by wave function engineering. These kinds of controls are not so possible in a single type-I or single type-II HNSs. We hope that this study will stimulate new experiments related to advanced wave function engineering studies in order to take cutting-edge device applications one step further.

## Declaration of competing interest

The authors declare that they have no known competing financial interests or personal relationships that could have appeared to influence the work reported in this paper.

## Data availability

No data was used for the research described in the article.

## References


[1] N Kirstaedter, OG Schmidt, NN Ledentsov, D Bimberg, VM Ustinov, A Yu Egorov, AE Zhukov, MV Maximov, PS Kop'ev, Zh I Alferov, Gain and differential gain of single layer inAs/Gaas quantum dot injection lasers, Appl. Phys. Lett. 69 (9) (1996) 1226–1228.

[2] Songtao Liu, Xinru Wu, Daehwan Jung, Justin C Norman, MJ Kennedy, Hon K Tsang, Arthur C Gossard, John E Bowers, High-channel-count 20 GHz passively mode-locked quantum dot laser directly grown on Si with 4.1 Tbit/s transmission capacity, Optica 6 (2) (2019) 128–134.

[3] Pegah Amini, Samiye Matloub, Ali Rostami, Multi-wavelength solution-processed quantum dot laser, Opt. Commun. 457 (2020) 124629.

[4] Polina O Anikeeva, Jonathan E Halpert, Moungi G Bawendi, Vladimir Bulovic, Quantum dot light-emitting devices with electroluminescence tunable over the entire visible spectrum, Nano Lett. 9 (7) (2009) 2532–2536.

[5] Junjie Hao, Haochen Liu, Jun Miao, Rui Lu, Ziming Zhou, Bingxin Zhao, Bin Xie, Jiaji Cheng, Kai Wang, Marie-Helene Delville, A facile route to synthesize CdSe/ZnS thick-shell quantum dots with precisely controlled green emission properties: towards QDs based LED applications, Sci. Rep. 9 (1) (2019) 1–8.

[6] Gencai Pan, Xue Bai, Wen Xu, Xu Chen, Yue Zhai, Jinyang Zhu, He Shao, Nan Ding, Lin Xu, Biao Dong, et al., Bright blue light emission of Ni2+ ion-doped CsPbCl x Br3–x Perovskite quantum dots enabling efficient light-emitting devices, ACS Appl. Mater. Interfaces 12 (12) (2020) 14195–14202.

[7] Matthew C Beard, Kelly P Knutsen, Pingrong Yu, Joseph M Luther, Qing Song, Wyatt K Metzger, Randy J Ellingson, Arthur J Nozik, Multiple exciton generation in colloidal silicon nanocrystals, Nano Lett. 7 (8) (2007) 2506–2512.

[8] Bin Sun, Oleksandr Voznyy, Hairen Tan, Philipp Stadler, Mengxia Liu, Grant Walters, Andrew H Proppe, Min Liu, James Fan, Taotao Zhuang, et al., Pseudohalide-exchanged quantum dot solids achieve record quantum efficiency in infrared photovoltaics, Adv. Mater. 29 (27) (2017) 1700749.

[9] Dong Liu, Jianqiang Liu, Jie Liu, Sha Liu, Chenglei Wang, Zhongwei Ge, Xiaotao Hao, Na Du, Hongdi Xiao, The photovoltaic performance of CdS/CdSe quantum dots co-sensitized solar cells based on zinc titanium mixed metal oxides, Physica E 115 (2020) 113669.

[10] Oliver T Bruns, Thomas S Bischof, Daniel K Harris, Daniel Franke, Yanxiang Shi, Lars Riedemann, Alexander Bartelt, Frank B Jaworski, Jessica A Carr, Christopher J Rowlands, et al., Next-generation in vivo optical imaging with short-wave infrared quantum dots, Nat. Biomed. Eng. 1 (4) (2017) 1–11.

[11] Jie Cao, Binling Zhu, Kefang Zheng, Songguo He, Liang Meng, Jibin Song, Huanghao Yang, Recent progress in NIR-II contrast agent for biological imaging, Front. Bioeng. Biotechnol. 7 (2020) 487.

[12] Maria C Tamargo, Igor L Kuskovsky, Carlos Meriles, Ismail C Noyan, Enhanced Materials Based on Submonolayer Type-II Quantum Dots, Tech. Rep., City College of New York, NY (United States), 2017.

[13] Arunav Bordoloi, Valentina Zannier, Lucia Sorba, Christian Schönenberger, Andreas Baumgartner, A double quantum dot spin valve, Commun. Phys. 3 (1) (2020) 1–7.

[14] S.D. Gunapala, B.F. Levine, L. Pfeiffer, K. West, Dependence of the performance of GaAs/AlGaAs quantum well infrared photodetectors on doping and bias, J. Appl. Phys. 69 (9) (1991) 6517–6520.

[15] RCC Leon, Chih Heng Yang, JCC Hwang, J Camirand Lemyre, Tuomo Tanttu, Wister Huang, Kok Wai Chan, KY Tan, FE Hudson, KM Itoh, et al., Coherent spin control of s-, p-, d-and f-electrons in a silicon quantum dot, Nature Commun. 11 (1) (2020) 1–7.

[16] Marina A Leontiadou, Edward J Tyrrell, Charles T Smith, Daniel Espinobarro-Velazquez, Robert Page, Jacek Miloszewski, Thomas Walsh, David Binks, Stanko Tomić, et al., Influence of elevated radiative lifetime on efficiency of CdSe/CdTe type II colloidal quantum dot based solar cells, Sol. Energy Mater. Sol. Cells 159 (2017) 657–663.

[17] S.A. Ivanov, M. Achermann, Spectral and dynamic properties of excitons and biexcitons in type-II semiconductor nanocrystals, Acs Nano 4 (10) (2010) 5994–6000.

[18] Fatih Koç, Koray Koksal, Mehmet Sahin, Effect of a buffer layer between the shell and ligand on the optical properties of an exciton and biexciton in type-II quantum dot nanocrystals, Phil. Mag. 97 (3) (2017) 201–211.

[19] Sunao Shimizu, Keiichiro Matsuki, Kazumoto Miwa, Daniele Braga, Shimpei Ono, Giant photo-induced current enhancement in a core–shell-type quantum-dot thin film, Adv. Electron. Mater. 6 (3) (2020) 1901069.

[20] Chengyuan Yan, Jiamin Wen, Peng Lin, Zhenhua Sun, A tunneling dielectric layer free floating gate nonvolatile memory employing type-I core–shell quantum dots as discrete charge-trapping/tunneling centers, Small 15 (1) (2019) 1804156.

[21] Zhan-Peng Wang, Yan Wang, Jinbo Yu, Jia-Qin Yang, Ye Zhou, Jing-Yu Mao, Ruopeng Wang, Xiaojin Zhao, Wenhan Zheng, Su-Ting Han, Type-I core–shell Znse/ZnS quantum dot-based resistive switching for implementing algorithm, Nano Lett. 20 (7) (2020) 5562–5569.

[22] Guiju Liu, Xiaohan Wang, Bingxu Liu, Guangting Han, Wei Jiang, Yuanming Zhang, Haiguang Zhao, Band engineering enables highly efficient and stable photoelectrochemical hydrogen evolution, Chem. Eng. J. 450 (2022) 137813.

[23] A Imamog, David D Awschalom, Guido Burkard, David P DiVincenzo, Daniel Loss, M Sherwin, A Small, et al., Quantum information processing using quantum dot spins and cavity QED, Phys. Rev. Lett. 83 (20) (1999) 4204.

[24] Jason R Petta, Alexander Comstock Johnson, Jacob M Taylor, Edward A Laird, Amir Yacoby, Mikhail D Lukin, Charles M Marcus, Micah P Hanson, Arthur C Gossard, Coherent manipulation of coupled electron spins in semiconductor quantum dots, Science 309 (5744) (2005) 2180–2184.

[25] F.H.L. Koppens, K.C. Nowack, LMK Vandersypen, Spin echo of a single electron spin in a quantum dot, Phys. Rev. Lett. 100 (23) (2008) 236802.

[26] Stanko Tomić, Jacek M. Miloszewski, Edward J. Tyrrell, David J Binks, Design of core/shell colloidal quantum dots for MEG solar cells, in: 2015 IEEE 42nd Photovoltaic Specialist Conference (PVSC), IEEE, 2015, pp. 1–4.

[27] Sungjee Kim, Brent Fisher, Hans-Jürgen Eisler, Moungi Bawendi, Type-II quantum dots: CdTe/CdSe (core/shell) and CdSe/ZnTe (core/shell) heterostructures, J. Am. Chem. Soc. 125 (38) (2003) 11466–11467.

[28] Huwei Feng, Jiaojiao Song, Bin Song, Qingli Lin, Huaibin Shen, Lin Song Li, Hongzhe Wang, Zuliang Du, Highly efficient near-infrared light-emitting diodes based on chloride treated CdTe/CdSe type-II quantum dots, Frontiers in Chemistry 8 (2020) 266.

[29] Masoomeh Taherkhani, Morten Willatzen, Emil V Denning, Igor E Protsenko, Niels Gregersen, High-fidelity optical quantum gates based on type-II double quantum dots in a nanowire, Phys. Rev. B 99 (16) (2019) 165305.

[30] Ahmet Emre Kavruk, Mehmet Sahin, Fatih Koc, Linear and nonlinear optical properties of G a A s/A lx G a 1- x A s/G a A s/A ly G a 1- y A s multi-shell spherical quantum dot, J. Appl. Phys. 114 (18) (2013) 183704.

[31] Ahmet Emre Kavruk, A detailed investigation of electronic and optical properties of single exciton in GaAs/AlxGa1-xAs/Gaas/AlyGa1-yAs multi-shell quantum dot, Phil. Mag. 98 (34) (2018) 3109–3125.

[32] Ahmet Emre Kavruk, Mehmet Sahin, Ülfet Atav, A detailed investigation of electronic and intersubband optical properties of AlxGa1- xAs/Al0. 3Ga0. 7As/AlyGa1- yAs/Al0. 3Ga0. 7As multi-shell quantum dots, J. Phys. D: Appl. Phys. 47 (29) (2014) 295302.

[33] Muharrem Kirak, Effects of electric and magnetic fields on the binding energy and second harmonic generation for on-and off-center donor impurities in spherical multilayer quantum dot, Eur. Phys. J. Plus 136 (6) (2021) 1–21.

[34] Kanghong Wang, Xin Tong, Yufeng Zhou, Hui Zhang, Fabiola Navarro-Pardo, Gurpreet S Selopal, Guiju Liu, Jie Tang, Yiqian Wang, Shuhui Sun, et al., Efficient solar-driven hydrogen generation using colloidal heterostructured quantum dots, J. Mater. Chem. A 7 (23) (2019) 14079–14088.

[35] Kanghong Wang, Yi Tao, Zikun Tang, Daniele Benetti, François Vidal, Haiguang Zhao, Federico Rosei, Xuhui Sun, Heterostructured core/gradient multi-shell quantum dots for high-performance and durable photoelectrochemical hydrogen generation, Nano Energy 100 (2022) 107524.

[36] Abdurrahman Aktürk, Mehmet Sahin, Fatih Koç, Ahmet Erdinc, A detailed investigation of electronic and optical properties of the exciton, the biexciton and charged excitons in a multi-shell quantum dot nanocrystal, J. Phys. D: Appl. Phys. 47 (28) (2014) 285301.

[37] Zhixin Song, Guangjun Xie, Xin Cheng, Lei Wang, Yongqiang Zhang, An ultra-low cost multilayer RAM in quantum-dot cellular automata, IEEE Trans. Circuits Syst. II 67 (12) (2020) 3397–3401.
[38] D.J. BenDaniel, C.B. Duke, Space-charge effects on electron tunneling, Phys. Rev. 152 (2) (1966) 683.
[39] Mehmet Şahin, Sedat Nizamoglu, Ozan Yerli, Hilmi Volkan Demir, Re-ordering orbitals of semiconductor multi-shell quantum dot-quantum well heteronanocrystals, J. Appl. Phys. 111 (2) (2012) 023713.
[40] Mehmet Şahin, Sedat Nizamoglu, A Emre Kavruk, Hilmi Volkan Demir, Self-consistent computation of electronic and optical properties of a single exciton in a spherical quantum dot via matrix diagonalization method, J. Appl. Phys. 106 (4) (2009) 043704.
[41] Takuma Tsuchiya, Biexcitons and charged excitons in quantum dots: A quantum Monte Carlo study, Physica E 7 (3–4) (2000) 470–474.
[42] Sergio Brovelli, Richard D Schaller, SA Crooker, Florencio García-Santamaría, Yongfen Chen, Ranjani Viswanatha, Jennifer A Hollingsworth, Han Htoon, Victor I Klimov, Nano-engineered electron–hole exchange interaction controls exciton dynamics in core–shell semiconductor nanocrystals, Nature Commun. 2 (1) (2011) 1–8.
[43] U.E.H. Laheld, G.T. Einevoll, Excitons in CdSe quantum dots, Phys. Rev. B 55 (8) (1997) 5184.
[44] Mehmet Sahin, Fatih Koç, A model for the recombination and radiative lifetime of trions and biexcitons in spherically shaped semiconductor nanocrystals, Appl. Phys. Lett. 102 (18) (2013) 183103.
[45] Marco Califano, Alberto Franceschetti, Alex Zunger, Lifetime and polarization of the radiative decay of excitons, biexcitons, and trions in CdSe nanocrystal quantum dots, Phys. Rev. B 75 (11) (2007) 115401.
[46] Benito Alén, José Bosch, Daniel Granados, Juan Martínez-Pastor, Jorge M García, Luisa González, Oscillator strength reduction induced by external electric fields in self-assembled quantum dots and rings, Phys. Rev. B 75 (4) (2007) 045319.
[47] Zaiping Zeng, Christos S Garoufalis, Andreas F Terzis, Sotirios Baskoutas, Linear and nonlinear optical properties of ZnO/ZnS and ZnS/ZnO core shell quantum dots: effects of shell thickness, impurity, and dielectric environment, J. Appl. Phys. 114 (2) (2013) 023510.
[48] Fatih Koc, Mehmet Sahin, Electronic and optical properties of single excitons and biexcitons in type-II quantum dot nanocrystals, J. Appl. Phys. 115 (19) (2014) 193701.
[49] Christos S Garoufalis, Zaiping Zeng, Gabriel Bester, Iosif Galanakis, David Hayrapetyan, Emmanuel Paspalakis, Sotirios Baskoutas, Excitons in ZnO quantum dots: The role of dielectric confinement, J. Phys. Chem. C 126 (5) (2022) 2833–2838.
[50] Otfried Madelung, Semiconductors: Data Handbook, Springer Science & Business Media, 2004.
[51] E.J. Tyrrell, J.M. Smith, Effective mass modeling of excitons in type-II quantum dot heterostructures, Phys. Rev. B 84 (16) (2011) 165328.
[52] Jagjit Nanda, Sergei A Ivanov, Marc Achermann, Ilya Bezel, Andrei Piryatinski, Victor I Klimov, Light amplification in the single-exciton regime using exciton-exciton repulsion in type-II nanocrystal quantum dots, J. Phys. Chem. C 111 (42) (2007) 15382–15390.
[53] Hiroshi Fujiyasu, Koji Mochizuki, A proposal for p-type ZnS1-x Se x–ZnTe superlattices, J. Appl. Phys. 57 (8) (1985) 2960–2962.
[54] D Sarkar, HP Van Der Meulen, JM Calleja, JM Becker, Rolf J Haug, Klaus Pierz, Phonons in in As/ Al As single quantum dots observed by optical emission, Phys. Rev. B 71 (8) (2005) 081302.
[55] S Rodt, A Schliwa, K Pötschke, F Guffarth, D Bimberg, Correlation of structural and few-particle properties of self-organized in As/ Ga As quantum dots, Phys. Rev. B 71 (15) (2005) 155325.
[56] C Bonati, MB Mohamed, D Tonti, G Zgrablic, S Haacke, F Van Mourik, M Chergui, Spectral and dynamical characterization of multiexcitons in colloidal CdSe semiconductor quantum dots, Phys. Rev. B 71 (20) (2005) 205317.
[57] Ke Gong, James E Martin, Lauren E Shea-Rohwer, Ping Lu, David F Kelley, Radiative lifetimes of zincblende CdSe/Cds quantum dots, J. Phys. Chem. C 119 (4) (2015) 2231–2238.
[58] Praket P. Jha, Philippe Guyot-Sionnest, Trion decay in colloidal quantum dots, ACS Nano 3 (4) (2009) 1011–1015.